RICE UNIVERSITY

Exploiting Channel Symmetry in Two-Way Channels

by

Justin A. Fritz

A THESIS SUBMITTED
IN PARTIAL FULFILLMENT OF THE
REQUIREMENTS FOR THE DEGREE

Master of Science

APPROVED, THESIS COMMITTEE:

Dr. Behnaam Aazhang, *Chair*
J.S. Abercrombie Professor of Electrical and Computer Engineering

Dr. Ashutosh Sabharwal
Assistant Professor, Electrical and Computer Engineering

Dr. Joseph R. Cavallaro
Professor of Electrical and Computer Engineering

HOUSTON, TEXAS

APRIL 2010

Abstract

Exploiting Channel Symmetry in Two-Way Channels

by

Justin A. Fritz

Wireless communication is frequently employed for the bi-directional exchange of information between devices with disparate capabilities. Mobile devices such as cellular phones and laptops are subject to stringent size weight and power constraints relative to the base stations or access points they communicate with. Asymmetry of constraints results in asymmetry of the cost of computation. This disparity in cost motivates efforts to shift signal processing such as channel estimation and equalization from cost sensitive devices to those with more relaxed constraints. In this work we develop a two-way training, channel estimation and precoding scheme that shifts all the computation involved in dealing with multiplicative channel gain as well as frequency selective channels to the base station. This work demonstrates the first tractable implementation of a precoding based transceiver scheme of this class on the Rice University Wireless Open Access Research Platform (WARP).

Acknowledgements

My committee members and advisor, Behnaam Aazhang, have been instrumental in preparing this work. Melissa Duarte Siddharth Gupta and Patrick Murphy helped make possible the implementation on the Rice University WARP platform. Gareth Middleton has been very helpful and supportive during my research and writing. To my wife Jamie, your unwavering support and encouragement has been invaluable. Thank you.

To my father: You were my first teacher, you continue to inspire me.

Contents

List of Figures

List of Tables

CHAPTER 1

Introduction and Motivation

1.1 Fading

Fading presents a significant engineering challenge for wireless communication. Fading is the result of reflectors and attenuators that are present in the terrestrial environment in which much of wireless communication occurs. The presence of reflectors cause multiple copies of a carrier-modulated signal to arrive at a receiving antenna each of them delayed by the propagation time from the transmitter to the reflector and then from the reflector to the receiver. These copies of the signal each arrive with different amplitude, phase and delay as a result of the different path they took from transmitter to receiver. The receiver sees the superposition of the multiple copies resulting in phase shifted, attenuated signal that is smeared in the time domain. Mobility of either the transmitter, receiver or any of the reflectors results in fading that varies in time.

Fading can be categorized as multipath or shadowing, flat or frequency selective and as fast or slow fading. Multipath fading is the result of reflector causing multiple copies of the signal to arrive at the receiver while shadowing is the result of attenuators or obstacles that block the signal from reaching the receiver. The behavior of a fading

channel in the frequency domain determines whether fading is characterized as flat or frequency selective. Simply put, flat fading occurs if fading has the same effect across the entire bandwidth of the signal. Similarly, behavior in time domain classifies fading as either slow or fast; with slow fading the channel remains the same for multiple symbols where as with fast fading each symbol experiences a new realization of the channel.

The evolution of wireless technology has led to ever increasing data rates. Increasing data rates have lead to increases in symbol rates and consequently increased bandwidth. The result of this evolution as it pertains to the fading channel is twofold, first, a given channel that may have been flat fading for low data rate communication becomes frequency selective as bandwidth increases, second, channels that appeared to be fast fading tend to look more like a slow fading channel as symbol rates increase. We are mindful of these trends when designing models for wireless communication and will consider in this work a frequency selective, slow fading channel.

1.2 Channel Symmetry

Studies of electromagnetic propagation have long suggested that the terrestrial wireless channel should be symmetric or, at least, very correlated [1]. In [2] and [3] perfect symmetry of the channel is assumed so that the downlink channel is known due to uplink training. However, symmetry has rarely been leveraged by practical systems, in part because while the propagation models suggest that channels should be symmetric observed channels in fact, rarely were. The observed lack of symmetry is partially explained by effects of transceivers radio frequency (RF) front ends as noted in [4]. Further investigation in [5] reveal several phenomenon that may break channel symmetry. Examples of conditions that break symmetry include Frequency division duplex (FDD) communications, different transmit and receive RF hardware,

asymmetric scattering geometry, polarization effects, and others. Thus while channel symmetry may exist in many scenarios practical systems must overcome the inherent asymmetry caused by RF front ends and adapt to provide reliable communication in the presence of the other phenomenon listed above.

1.3 Two-way nature of modern communications

Modern communication systems are inherently two-way [6]. The two-way nature is apparent in cases such as cellar voice where both parties involved in point to point communication wish to transmit data. In many cases where data transfer is one way feedback such as acknowledgements and requests for data require a reverse link. This reverse link is of key importance to providing channel state information to the transmitter (CSIT). If the forward and reverse links were symmetric then channel state information at the receiver (CSIR) of the reverse link would be identical to CSIT for the forward link. Even with asymmetry as a result of the phenomenon listed in the previous section exploiting a relationship between the forward and backward link allows more efficient use of the channel in general.

Two-way communication where both stations are simultaneously broadcasting in the same band are not practical because of the large disparity between transmit and receive power[7]. With an eye towards practical systems we focus our attention on time division duplex (TDD) communication. This choice, not coincidently, alleviates a major cause of channel asymmetry found in FDD communication schemes.

1.4 Size, weight and power constraints (SWaP)

Yet another commonly observed feature of modern wireless communications systems is the asymmetry of size, weight and power (SWaP) constraints placed on devices in the system. Cellular systems are a classic example of a systems with asymmetric

constraints. The wireless portion of the classical cellular system consists of point-to-point communication of mobile devices to base stations. The mobile devices are small, battery operated devices; their utility is directly related to their form factor and battery life leading to stringent SWaP constraints. The base stations on the other hand are not mobile and obtain power from the electric power distribution grid leading to lax constraints relative to the mobile devices. Asymmetric constraints are observed in many other systems including laptops communicating with wireless access points and many others.

The cost of computation is directly related to the constraints placed on the device performing the calculations, that is, all else being equal, the cost of executing an algorithm is directly related to SWaP constraints. This motivates a review of the classical communications system. Engineering decisions are often an attempt to optimize system parameters in the face of a rich multivariate set of constraints. One down link system that performs well in terms of bit error rate (BER) in the presence of frequency selective fading is one which employs an equalizer at the receiver to mitigate inter symbol interference (ISI) [7]. If, however, the channel is known at the transmitter then precoding at the transmitter may provide the same ISI mitigation performance while reducing the computational burden at the mobile station.

1.5 Problem statement and approach

In this work we propose a training and precoding protocol to efficiently estimate and precode for the downlink channel. The training protocol exploits channel symmetry between antennas when it does exist and makes use of the slow variation of the transmitter and receiver RF front end impulse response relative to the air interface. When there is no symmetry the training protocol degrades to that of [5] for the MISO case. This training differs from that presented in [5] by interleaving up-link training

between round-trip training resulting in less overhead by exploiting the symmetric nature of the wireless channel. A zero forcing precoder is presented that alleviates the need for equalization at the receiver. This precoder shifts the computational cost of calculating a channel estimate and combating ISI in the downlink channel from the mobile station to the base-station.

A study of channel properties in an indoor, office environment is presented. Empirical results for two-way communication in the 2.4GHz ISM band are presented that show highly symmetric channel conditions and very slow changing RF impulse responses occur in laboratory and office environments.

A test system implementing the two-way training and precoding protocol are compared against systems employing differential quadrature amplitude modulation (DQAM) a and the Alamouti scheme. The computational complexity at the mobile receiver and bit error rate are used as metrics. This work shows that the two-way training and precoding protocol yield significant performance improvements over DQAM while maintaining low receiver complexity typically found in non coherent receivers. Succinctly, we show that this protocol outperforms current systems with identical complexity at the receiver.

We consider a downlink that is constrained by a per antenna power constraint. This choice of constraints was motivated by first noting that the base station has relaxed power constraints lifting the total power constraint and second, by noting that the cost of RF power amplifiers is strongly correlated with peak power output resulting in many systems that are, indeed constrained in this manner [8].

The system of interest in this work is a uncoded, fixed rate system. When considering this type of system bit error rate is a logical metric to measure performance. For an empirical study of a system BER is a progenitor of many other metrics used to evaluate communications systems. Given a distribution on the fading channel and coding overhead BER can be mapped to probability of outage. Given BER,

bandwidth and fraction of channel usage committed to training overhead the spectral efficiency of the protocol provided here can be calculated.

CHAPTER 2

Channel Model

2.1 Model

We consider the frequency selective, composite, TDD two-way, MISO channel pictured in figure 2.1. For the baseband model we assume perfect modulation/demodulation and quantization of the carrier modulated signal. Due to the size weight and power constraints we assume that the base station has $M > 1$ antennas and the mobile station possesses 1 antenna. In this model the base station is represented by $\mathcal{A}$ and the mobile station by $\mathcal{B}$. The channel impulse responses (CIRs) of the analog front ends are denoted by T_A and t_B for the transmitter chain while the receiver CIRs are denoted by R_A and r_B. Subscripts refer to the transceiver associated with the CIR.

The sampled frequency selective channel is represented as a linear, time varying filter in the time domain. T_A and R_A are both $M \times M$ matrices where the diagonal components represent single antenna impulse responses. Very little cross-talk was observed in the laboratory and modern RF front ends have little cross talk by design [9] leading us to assume that both T_A and R_A are diagonal.

The forward fading channel $\vec{h}(\tau)$ is the composite channel consisting of the base station transmitter, the wireless channel and the mobile's receiver. This composite

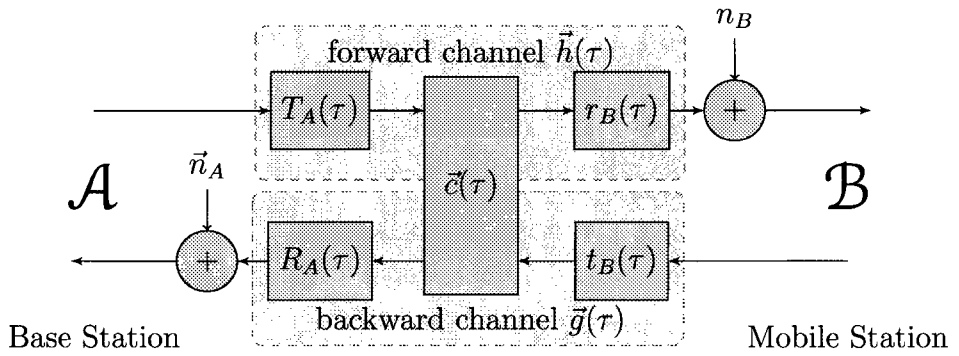

Figure 2.1: Composite channel model block diagram

channel is given by

$$\vec{h}(\tau) = r_B(\tau) * \vec{c}(\tau)^T * T_A(\tau) \tag{2.1}$$

where $*$ represents linear convolution across the lag index τ. Similarly, the reverse channel is given by

$$\vec{g}(\tau) = R_A(\tau) * \vec{c}(\tau) * t_B(\tau). \tag{2.2}$$

The sampled, frequency selective channel is represented as a time varying finite impulse response (FIR) filter by truncating the theoretically infinite impulse response of the wireless channel and RF front ends. The wireless channel $\vec{c}(\tau)$ consists of L_c pertinent taps while the CIR for the RF front ends consist of L_x taps. The resulting composite channel will consist of $L = L_c + 2L_x - 2$ taps. We note that $\vec{h}(\tau) \in \mathbb{C}^{M\times 1\times L}$ and $\vec{h}(\tau) \in \mathbb{C}^{1\times M\times L}$. The complete channel model can be written as

$$y_{AB} = \sum_{i=1}^{M} (\vec{h}(\tau) * \vec{x}_A(\tau)) + n(\tau) \tag{2.3}$$

for the forward channel where the summation is over the antenna pairs and

$$\vec{y}_{BA} = \vec{g}(\tau) * \vec{x}_B(\tau) + \vec{n}(\tau) \tag{2.4}$$

for the backward channel.

2.2 Variation in Time

The model presented in the previous section provides a snapshot of the channel in time; in this section we outline a model to capture the effects of the time varying channel.

2.2.1 Per Symbol Variation

Here we model the Rayleigh fading wireless channel $\vec{c}$ as an AR1 auto regressive random process. Antenna pairs are assumed uncorrelated and taps in the frequency selective model are assumed uncorrelated. With theses assumptions we have

$$c_i(\tau)[k] = \alpha c_i(\tau)[k-1] + z_i(\tau)[k], \qquad 0 \leq \alpha \leq 1 \tag{2.5}$$

for $i \in 1, 2, ..., M$ and $\tau \in 0, 1, ..., L-1$. Maintaining an average channel gain of unity we have $c_i \sim \mathbb{CN}(0, \frac{2}{\pi})$ and $z_i \sim \mathbb{CN}(0, \frac{2}{\pi}(1-\alpha))$ for flat fading while for the frequency selective channel $E\left[\sum_{\tau=0}^{L-1} |c_i(\tau)|\right] = 1$. Equation 2.5 characterizes the wireless channel as a Gauss–Markov process in which the components of the channel impulse response experience a circularly symmetric Gaussian random walk over the complex plane.

While the Gauss-Markov model has been shown to be a reasonable model for the evolving Rayleigh channel [10] this model is a poor fit for the RF front ends. In WARP experiments the RF front ends appear to be best modeled as a constant gain and time varying phase rotation. This phase rotation consists of an initial rotation, frequency offset and jitter. Clock jitter is often modeled as a Gaussian random walk about the unit circle. Since phase offset between different antennas on the same transceiver make no difference to our analysis we can compactly represent the RF front ends as follows

$$T_A[k] = e^{j(\Delta k + x_2\phi[k-1]+q'[k])} \begin{bmatrix} Ae^{j\theta_1} & 0 & \cdots & 0 \\ 0 & Ae^{j\theta_2} & & \vdots \\ \vdots & & \ddots & 0 \\ 0 & \cdots & 0 & Ae^{j\theta_M} \end{bmatrix}. \tag{2.6}$$

In Equation 2.6 Δ is the frequency offset, ϕ is the jitter term, $q' \sim \mathbb{CN}(0, (1-\alpha_2)\sigma_\phi)$, $A_1, A_2, ..., A_M$ are the individual gains and $\theta_1, \theta_2, ..., \theta_M$ are the initial phase rotations. The other terms representing RF front ends $R_A[k]$, $t_A[k]$ and $r_B[k]$ all take the same form.

Since the gains are adjustable they can be set such that $A_1 = A_2 = .. = A_M$ allowing us to normalize the gain in the model. In addition we note that the the phase difference between antennas may be omitted and Equation 2.6 can be simplified to

$$T_A[k] = e^{j(\Delta k + x_2\phi[k-1]+q'[k])} I_M. \tag{2.7}$$

The end result of this model is a Gauss-Markov channel that is symmetric up to a phase rotation. The phase rotations commute and the difference between the forward and reverse channel can be grouped into a single term as pictured in Figure 2.2. In the commuted composite channel model the forward channel model is given by

$$\vec{h} = H'(\tau) * \vec{g}(\tau) \tag{2.8}$$

where H' is a $M \times M$ diagonal matrix with diagonal terms $h_i'[k] = e^{j(\alpha_3\phi[k-1]+q[k])}$. Elements of $\vec{g}$ are described by $g_i[k] = (\alpha g_i[k-1] + z[k])e^{j(\alpha_3\phi[k-1]+q[k])}$. In words this

is a Gauss-Markov channel model that evolves with an independent rotation applied to the forward and backward channels.

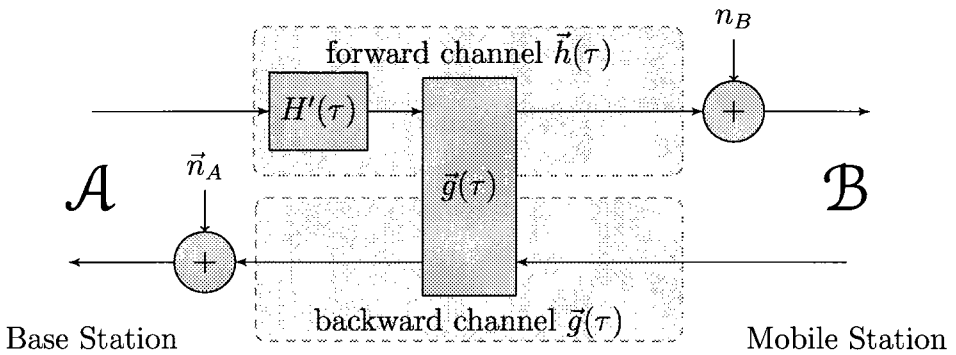

Figure 2.2: Commuted composite channel model block diagram

2.2.2 Block-fading Model

The block-fading model has enjoyed widespread use in publications such as [11, 12] and others. This model applies to channels where the time varying fading changes so little that it can be assumed invariant for a block of symbols. Block-fading can be viewed as a simplification of the per symbol variation model given two conditions. First, the block must be sufficiently short such that the channel does not change significantly for a give modulation scheme with high probability. Second, the systems we wish to analyze must not maintain memory beyond the block of channel symbols.

For the case in question in this thesis we present a block fading model in which the wireless channel $\vec{c}$ is composed of i.i.d. random variables c_i, $i \in 1, 2, ..., M$ with $c_i \sim \mathbb{CN}(0, \frac{2}{\pi})$ for an average unity channel gain per antenna pair. All elements of $\vec{c}$ are drawn at an interval of T_c symbol times. The diagonal elements of R_A and T_A as well as t_B and r_B are of the form $A_i e^{j\phi_i}$ with $\phi_i \sim \mathcal{U}(0, 2\pi)$. All ϕ_i's are drawn at an interval of T_{RF} symbol times. The coherence time of the RF components is assumed to be much longer than that of the wireless channel therefor $T_{RF} = nT_c$ where $n \in \mathbb{Z}^+$ and $n \gg 1$.

This block fading model differs from those commonly seen in literature by way of having two coherence times. This is born out of empirical data collected from the WARP radio system that demonstrates a symmetric wireless channel that experiences a slow asymmetric phase rotation between the forward and reverse channel. With this new model in hand we will develop a channel training, estimation and precoding scheme in the subsequent chapters that takes advantage of the disparate coherence times of the wireless channel and the RF front ends. Furthermore, we will present results to validate the assumptions used in devising this model.

CHAPTER 3

Channel Training and Estimation

3.1 Phase Coherent Communication

Practical communication in the fading channel can be partitioned in to two classes, those that are phase coherent and those that are not. Many modern systems utilize phase coherent schemes due to a 3dB gain over non-coherent schemes at a cost of increased complexity particularly at the receiver [13]. For devices that operate under strict SWaP constraints this trade off forces non coherent communication such as the use of DPSK in the Bluetooth personal area network specification. Phase coherent systems may be further subdivided into ones that derive a carrier reference from a pilot signal multiplexed with modulated data and ones that obtain a reference directly from the modulated data. The former method of obtaining a phase reference is widely utilized, appearing in standards including 802.11, GSM and others [14]. In this section we provide background by first exploring phase coherent communication in a one-way channel and then build up to the two-way channel.

Consider a simple, flat fading channel with AWGN modeled by $y = hx + n$. The complex, noisy, demodulated data symbol has been multiplied by the complex valued channel gain h. Without more information a receiver is unable to determine what

symbol was sent when modulation schemes such as phase shift keying (PSK) and quadrature amplitude modulation (QAM) are utilized. The receiver must know, or in reality estimate the phase of h for PSK as well as the magnitude for QAM. This estimate of the channel may be obtained by sending a training symbol, for the sake of simplicity set the training as $y = h1 + n$. The receiver may obtain an efficient estimate $\hat{h} = y$. So long as the channel remains constant (we assume slow fading) subsequent data symbols may be estimated by first inverting the channel effect and then mapping it to the closest valid symbol as follows.

$$\hat{x} = \underset{x}{\text{argmax}} \left|\left| x - \frac{y}{\hat{h}} \right|\right| \tag{3.1}$$

Our simple estimate of h considers only one training symbol and makes no assumption of the statistics of the channel. Since the channel is flat fading the single tone, that is the carrier modulated by unity is sufficient. For estimates formed from k pilot symbols our simple estimate may be extended to $\frac{1}{k}\sum_{i=0}^{k-1} y$. Estimation that account for prior distributions are treated in [15] and estimators with the wireless channel specifically in mind have been the focus of much research. We will investigate LS estimates for the frequency selective channel next but will not treat the more advanced MMSE estimates that consider prior distributions. We exclude treatment of this class of estimates for two reasons. First, the results presented later serve as a lower bound on performance and second, the least squares estimate allows for a feasible implementation.

The steps of inverting the effect of the fading channel and estimating a data symbol are outlined in Figure 3.1. The receiver first attempts to remove the phase rotation and scaling of received symbol by diving the symbol by the channel estimate. The receiver then form an estimate of the data symbol by mapping it to the closest valid

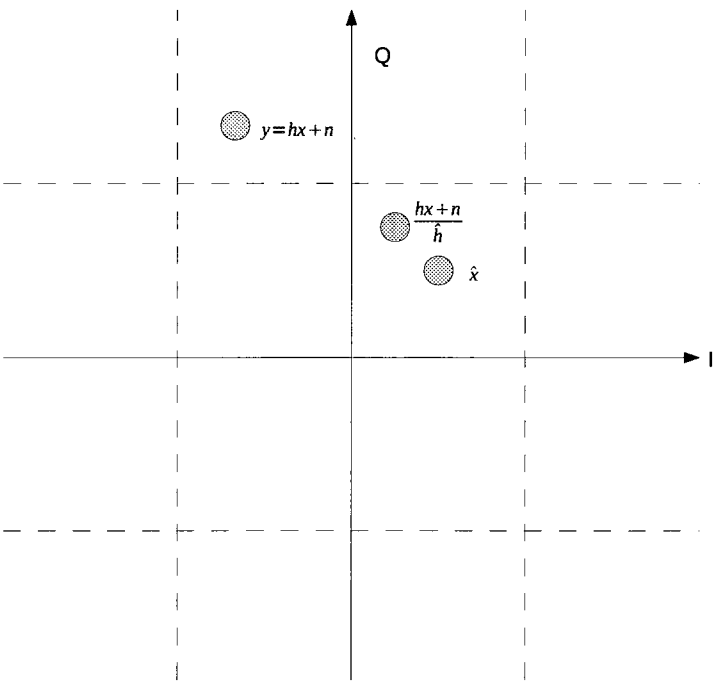

Figure 3.1: Inverting the channel effect and estimating a data symbol

symbol.

A receiver operating in the above fashion that encounters the frequency selective channel given in Equation 2.3 must invert the channel to remove the effects of ISI. For a channel consisting of L taps the training based channel estimate can be derived from the minimum sufficient statistic of L training symbols. The forward channel cascaded with an equalizer takes the form $h_o(\tau) = \sum_{i=0}^{M} \vec{h_i}(\tau) * h_E(\tau)$.

Carrier frequency CFO offset is a parameter of the received signal that must be estimated. A thorough analysis of carrier recovery is provided in [13]. It suffices to say for a training based estimate the minimum length training sequence must be increased by one to $L+1$. A received training sequence $R[k]$, $k \in 1, 2, ..., L+1$ in the presence of CFO takes on the form

$$R[k] + e^{j2\pi k\Delta} \tag{3.2}$$

where Δ is per symbol phase rotation induced by CFO.

3.2 Training for the Two-way Channel

The training protocol we specify consists of two different training sequences, round trip training (RTT) and uplink training (UT). The round trip training sequence is utilized to provide sufficient statistics to the base-station for an estimate of the forward channel $\hat{h}$ and the reverse channel $\hat{g}$.

RTT is completed by the following sequence of events. In the first step training is sent from the base-station to the mobile station, this step is referred to as forward training. This training sequence occupies the full bandwidth of the channel, consists of orthogonal signals from each of the M transmit antennas at the base station, and is sufficient in duration that the frequency selective channel may be determined. A sufficient statistic for a SISO frequency selective channel consisting of L taps is the received waveform for at least L training symbols. Since training between antenna pairs in the MISO case is orthogonal a total of LM training symbols is needed for the first phase of training. The mobile station buffers the received waveform from the first step of RTT and in the second step, called return training, transmits the buffered copy of the received waveform. The second step requires a total of LM training symbols. The third step of RTT is reverse training, in this step, training is sent from the mobile station to the base station. L training symbols are required for this phase of training.

UT is accomplished by sending sufficient training from the mobile to the base-station to derive an estimate for each of the mobile to base-station antenna pairs. In the SIMO uplink channel a single sequence of L training symbols is sufficient since this sequence is received by all of the receiver antennas allowing an estimate of all

antenna pairs.

for *each training interval* **do**

  if *RF coherence interval elapsed* **then** /* overhead $= LM$ */

    Forward training from Alice to Bob: $\vec{t}_{AB} = \vec{h} I_M + \vec{n}$ comment;

    Return training: $T_{ABA} = GX_E + N$;

    Reverse training from Bob to Alice: $\vec{t}_{BA} = G1^{M\times 1} + \vec{n}$;

  else /* overhead $= L$ */

    Reverse training from Bob to Alice: $\vec{t}_{BA} = G1^{M\times 1} + \vec{n}$;

  end

end

Algorithm 1: Training algorithm

After RTT has been performed the base-station possesses T_{ABA} and $\vec{t}_{BA}$. T_{ABA} is training that has passed through the cascade of the forward and reverse channel and is sufficient for the estimate $\widehat{h * g}$ while $\vec{t}_{BA}$ may be used to form the estimate $\hat{g}$. The least squares method of estimation for $\widehat{h * g}$ and $\hat{g}$ provides a minimum variance, unbiased (MVU) estimate and attains the Cramér-Rao bound resulting in an efficient estimate. An efficient estimate for the forward channel is desired however the information at the transmitter yields an MVU estimate that does not attain the Cramér-Rao bound.

The estimates for the forward and backward channel are given by

$$\hat{g} = T_{BA} X_b^{+} \tag{3.3}$$

$$\hat{h} = g^{+} y_{ABA} X_A^{+} \tag{3.4}$$

3.3 Comparison of Training Costs

In this section we compare the cost as a fraction of channel symbols of the two-way training protocol with that of separate one-way training protocols. Given the commutated, frequency selective, block fading model presented in Chapter 2 the symmetric portion of the channel has a coherence time of $T_c = nT_s$ seconds and the asymmetric portion a coherence time of $T_{RF} = kT_c = knt_s$ where $k, n \in \mathbb{Z}^+$ and t_s is the duration of one symbol.

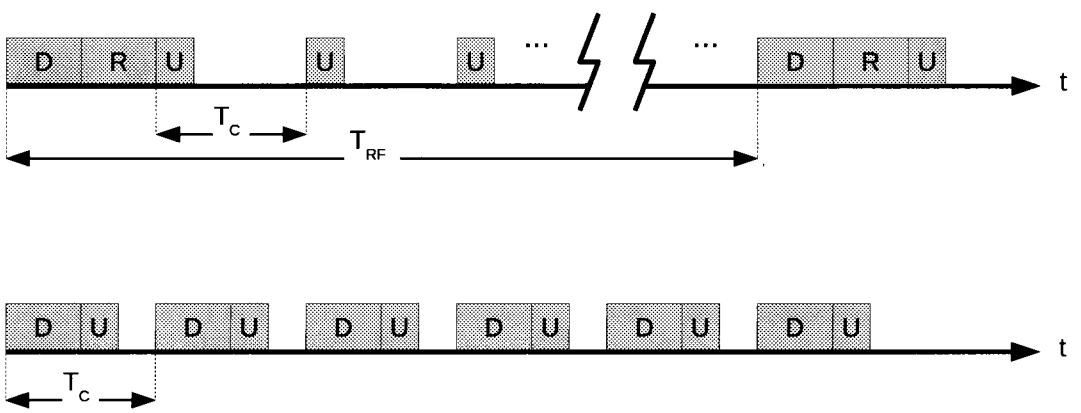

Figure 3.2: Time-line for two-way and one-way training

First we compute the cost of training for the two-way training protocol. A time-line depicting the training sequence is presented in Figure 3.2 where it is observed that the two-way protocol is periodic with period T_{RF}. During this time forward and reverse training are performed once while uplink training is performed k times for a

total of $L(2M + k)$ training symbols per period. Division by the period yields the fraction of channel usage for the two-way protocol

$$p_2 = \frac{L(2M + k)}{kn}. \tag{3.5}$$

One way training is unable to leverage the slow varying nature of the asymmetric portion of the channel and must therefore transmit both forward and reverse training during the coherence time of the channel. This training pattern is periodic with period T_C and leads to $L(1+M)$ training symbols per period. Therefore the one-way protocol utilizes

$$p_1 = \frac{L(1 + M)}{n}. \tag{3.6}$$

fraction of the symbol times for training.

Examination of the expressions of training time we note that as the number of antennas M and channel length L grow the fraction devoted to training grows. Where the two-way training shows gains is when T_{RF} is much larger than T_C which is often the case as we will soon see.

Previous works have solved for the optimal training interval by maximizing an achievable rate expression [16],[17]. While this yields an analytical solution this solution is not of practical use. For the implementation we consider a TDD system in which the uplink and downlink frames are of fixed duration and uplink training is performed on each uplink frame. This leaves only the round trip training period to adjust. During experiments presented in this work the transmitted data was known a-priori at the mobile station. With this a-priori knowledge the mobile station in

the test system is able to determine BER in real time and signal the base station to retrain when the BER falls below a threshold. In a coded system retraining could be initiated upon reaching a threshold in decoding errors.

CHAPTER 4

Precoding

Precoding systems take on many forms, the multi-antenna transmitter may perform beamforming to increase SNR at a receiver [18], MIMO transceivers may achieve a multiplexing gain by decomposing the MIMO channel into orthogonal sub-channels [19] or precoding may be used to reduce complexity at the receiver [20]. We examine precoding as a means to reduce complexity at the receiver, specifically faced with the problem of frequency selective slow fading we explore precoding that takes the place of equalization. Furthermore, in the MISO system we present simulation and experimental results that show that full diversity can be achieved with simple precoding and show that our precoding scheme provided with perfect CSIT achieves a 3dB gain over the Alamouti scheme with perfect CSIR.

4.1 Flat Fading

Precoding for the flat fading channel is used as a stepping stone for frequency selective channels. In this case the the estimate $\hat{h}$ of the forward channel at the base-station is a $1 \times M$ vector. Full diversity of the MISO system is achieved if the signals arrive at the receive antenna such that they add constructively. If the phase rotation imparted by each antenna pair were known then the precoder that achieves full diversity simply

inverts the rotation imparted by each antenna pair. Since only estimates of phase rotation are available there is a penalty as will be observed in the results section.

Given a fixed transmit power for each antenna the diversity achieving per symbol precoding is simply a rotation that is inverse to that imparted by the channel for each antenna pair. With the estimate $\hat{h}$ the base-station forms the precoding vector

$$\vec{p} = \left[e^{-j\angle\hat{h}_1}, e^{-j\angle\hat{h}_2}, ..., e^{-j\angle\hat{h}_M}\right] \tag{4.1}$$

where $\angle\hat{h}_i$ is the estimated phase rotation induced by the i_{th} antenna pair. The resulting output at the receive is

$$y_{AB} = \vec{h}X\vec{p} + n \tag{4.2}$$

with $X = \frac{x}{M}I_M$. From this equation it is easy to see that if the estimated phase were perfect the received signal would be the input symbol times the sum of the channel gains plus noise, yielding full diversity.

Our treatment of the flat fading channel so far has only considered the phase imparted by the channel. This would be sufficient if we restrict modulation to PSK however, for QAM modulation the magnitude of the channel must also be considered. In this case we have precoding given by

$$\vec{p} = \left[\alpha_1 e^{-j\angle\hat{h}_1}, \alpha_2 e^{-j\angle\hat{h}_2}, ..., \alpha_M e^{-j\angle\hat{h}_M}\right] \tag{4.3}$$

and wish to solve for $\vec{\alpha}$

$$\vec{h}^T\vec{p} = 1$$

$$s.t. \alpha_1, \alpha_2, ..., \alpha_M \leq P \quad (4.4)$$

where P is the per antenna power constraint. It is easy to show that water filling across the antennas is optimal in terms of total power consumption. For the implementation presented below we set our precoding vector to

$$\vec{p} = \frac{1}{\left|\left|\hat{\vec{h}}\right|\right|}\left[e^{-j\angle\hat{h}_1}, e^{-j\angle\hat{h}_2}, ..., e^{-j\angle\hat{h}_M}\right] \quad (4.5)$$

up to the per antenna power constraint P. By selecting this sub optimal precoding scheme the results presented in this work represent a lower bound on the performance of the precoded system.

4.2 Frequency Selective Channels

The frequency selective channel presents a further challenge to the precoder at it causes ISI. In this section the zero forcing equalizer is presented. This architecture that is normally employed at the receiver may be instantiated at the transmitter instead by noting that both the channel and the equalizer may be represented by linear filters and therefore, their order may be commuted. Finally we observe that each of the cascaded zero forcing precoders and channels represent a flat fading channel allowing diversity maximizing precoding as presented in the previous section.

Consider the cascade of the forward channel and equalizer given in the frequency domain by

$$H_o(f) = H(f)E(f) \tag{4.6}$$

We wish to develop an equalizer that results in zero ISI, which is realized if Nyquist's first criterion is satisfied implying

$$\sum_{k=-\infty}^{\infty} H_o\left(f + \frac{t}{T_b}\right) = constant, |f| \leq \frac{1}{2T_b} \tag{4.7}$$

where the output of the equalizer is sampled every T_b seconds. from Equation 4.7 it follows that the ideal zero ISI equalizer is simply the inverse filter, which has a frequency response that is the inverse of the frequency response of the cascaded forward channel folded about the sampling frequency. A practical feed-forward filter or finite-impulse response filter can approximate this inverse filter since real channels posses a finite delay spread. The frequency response of this filter is given by

$$E(f) \sum_{n=-N}^{N} C_n e^{-j2\pi nfT_b} \tag{4.8}$$

Where C_n is the tap weights for the desired filter. The pulse response of the cascade of the channel and the equalizer is simply convolution given by

$$p_{eq}(t) = \sum_{n=-N}^{N} C_n p_c(t - nT_b) \tag{4.9}$$

where p_c is the pulse response observed at the output of the channel. The pulse response at the output of this cascade of filters should be one for exactly one symbol

time and zero elsewhere to satisfy zero ISI. This can be rewritten in matrix form as

$$\vec{p}_{eq} = P_C \vec{c} \tag{4.10}$$

where $\vec{p}_{eq}$ is the $1 \times (2N+1)$ column vector consisting of zeros excluding the $N+1_{th}$ element $p_{eq}(N+1) = 1$, $\vec{c}$ is the desired equalizer filter weights and P_C is the $(2N+1) \times (2N+1)$ matrix of channel filter taps of the form

$$P_C = \begin{bmatrix} p_C(t_d) & p_C(-T_B + t_d) & \cdots & p_C(-2NT_B + t_d) \\ p_C(T_b + t_d) & p_C(t_d) & \cdots & p_C[(-2N+1)T_B + t_d] \\ p_C(2T_b + t_d) & p_C(T_b + t_d) & \cdots & p_C[(-2N+2)T_B + t_d] \\ \vdots & \vdots & \ddots & \vdots \\ p_C(2NT_b + t_d) & p_C[(2N-1)T_B + t_d] & \cdots & Ae^{j\theta_M} \end{bmatrix}. \tag{4.11}$$

Note that in the above matrix t_d is the delay through the cascaded filter. Solving the above equation for the equalizer filter weights yields $\vec{c} = P_C^{-1} P_{eq}$. This equalizer requires $4N+1$ samples of the channel impulse response estimate to determine the $2N+1$ unknown coefficients.

With the zero forcing equalizer developed it is easy to see that substitution of terms in Equation 4.9 allows the order of the filters to be swapped turning our zero forcing equalizer into a precoder. Considering a MISO system the result is a separate zero forcing precoder for each antenna pair. The cascaded zero forcing precoder and frequency selective channel appear as the flat fading channel treated in Section 4.1. This system may then be precoded by a per antenna phase rotation to achieve diversity. The complete precoder system is pictured in Figure 4.1.

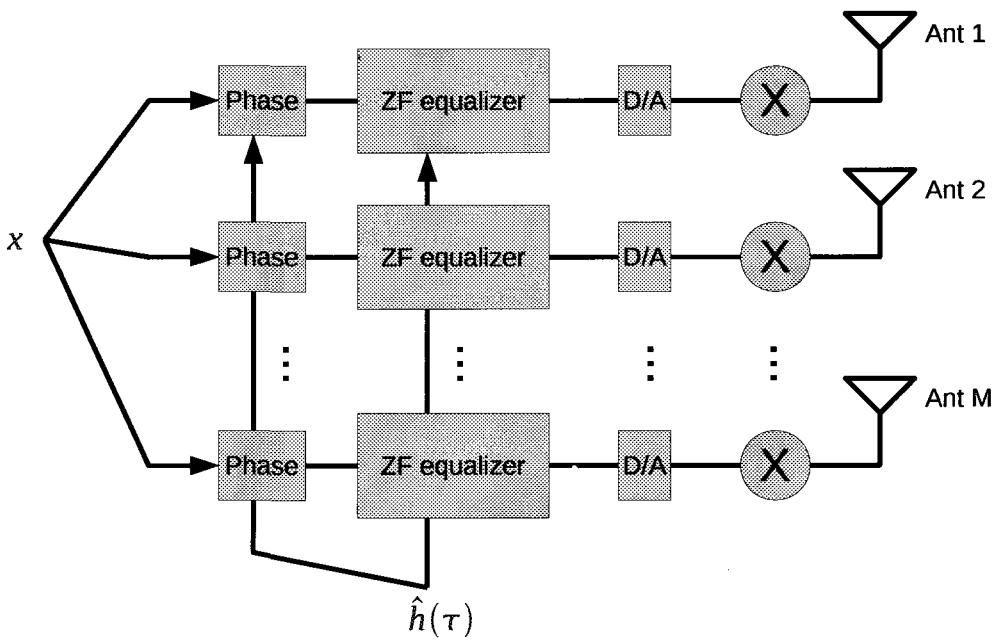

Figure 4.1: Zero-forcing precoder design

CHAPTER 5

Hardware Implementation

In the previous two chapters we developed a two-way training protocol and precoder. The training protocol provided the sufficient statistics at the base station to form estimates of the forward and reverse channels and the precoder mitigated the effects of ISI in the frequency selective channel and achieved diversity gain of M for a $M \times 1$ MISO channel. We now seek to demonstrate the feasibility of the precoder which is set by the estimates formed from the two way training protocol.

In this chapter we outline the WARPLab research framework and present a hardware implementation of the two way training and precoder called EchoWARPLab. This implementation uses WARPLab as a starting point however, significant hardware modifications were necessary. The system that is implemented includes a channel estimator for a two tap wireless channel, a three tap zero-forcing equalizer cascaded with a beamforming precoder. Finally, device utilization statistics are provided for this particular implementation and for higher order filters and estimators.

5.1 Hardware design

The hardware system presented here is based of the Rice University WARPLab Version 4, 2×2 MIMO system [21]. WARPLab allows real time transmission of up to

16384 complex valued samples at a sampling rate of 40 MHz modulated on either the 2.4 GHz or 5 GHz ISM band. For this work we have selected the parameters listed in Table 5.1.

Table 5.1: WARPLab radio parameters

Parameter	**Value**
Sampling frequency	40MHz
Carrier frequency	2.4GHz
Modulation	16 QAM
Symbol rate	1/4 symbol/sample

A top level diagram of the hardware model is shown in Figure 5.1. This model represents a custom hardware design that is implemented on the FPGA present on the WARP radio board. In this configuration one can configure the warp radio as either a transmitter or receiver then upload a vector of samples to the transmitter and finally, send a synchronization signal simultaneously to all radios commanding them to begin transmission or reception. Once the transmission cycle is complete the vector of received samples may be downloaded to the host computer for offline processing.

The training and precoding schemes that we propose require sending multiple signals between a base station and receiver before a data exchange takes place and were developed to operate in a slow fading channel. Furthermore, in order to precode for carrier frequency offset the timing of training and data symbols must be very tightly controlled. Having a host computer controlling the sending and receipt of packets results in an excessive and random delay in the time needed to reconfigure WARPLab from a transmitter to a receiver or vice-versa. In order to achieve quick, deterministic time reconfiguration of the radios we developed the hardware design to be described here.

A top level diagram of the EchoWARPLab hardware design is shown in Figure 5.2. For ease of development and testing the hardware for both the base station and

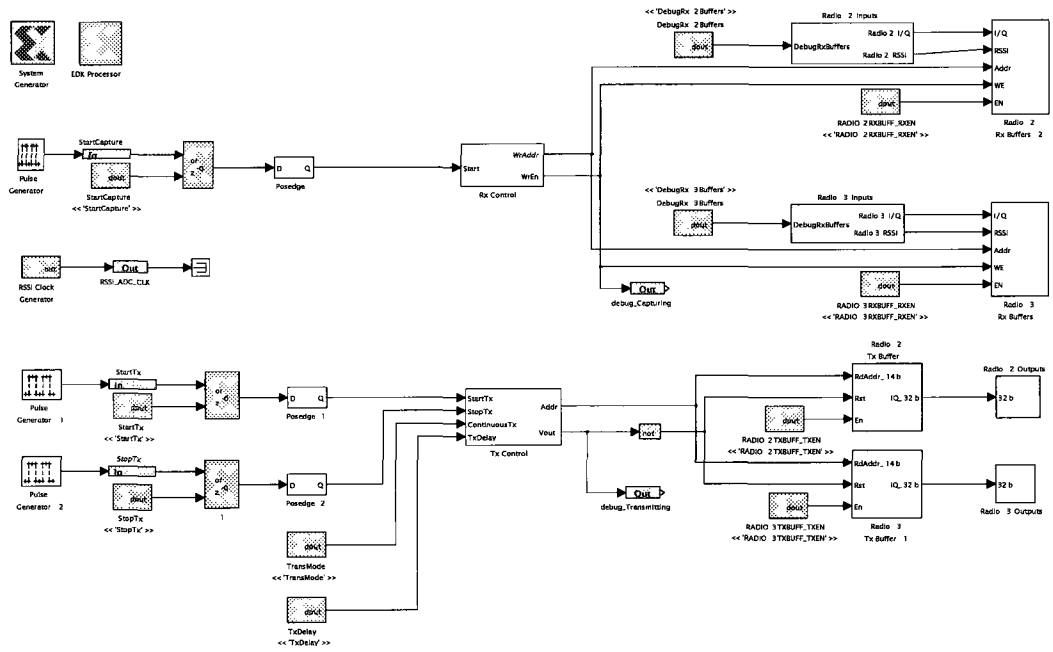

Figure 5.1: Top level WARPLab 2x2 hardware design

mobile station are included in one design, however the device utilization numbers are presented for an architecture consisting of only one or the other. The base station hardware consists of the following devices

- State machine
- Channel estimate
- precoder

while the mobile station hardware is made up of the following

- State machine
- Symbol/carrier synchronizer

- Hard decision
- BER counter and SNR estimator.

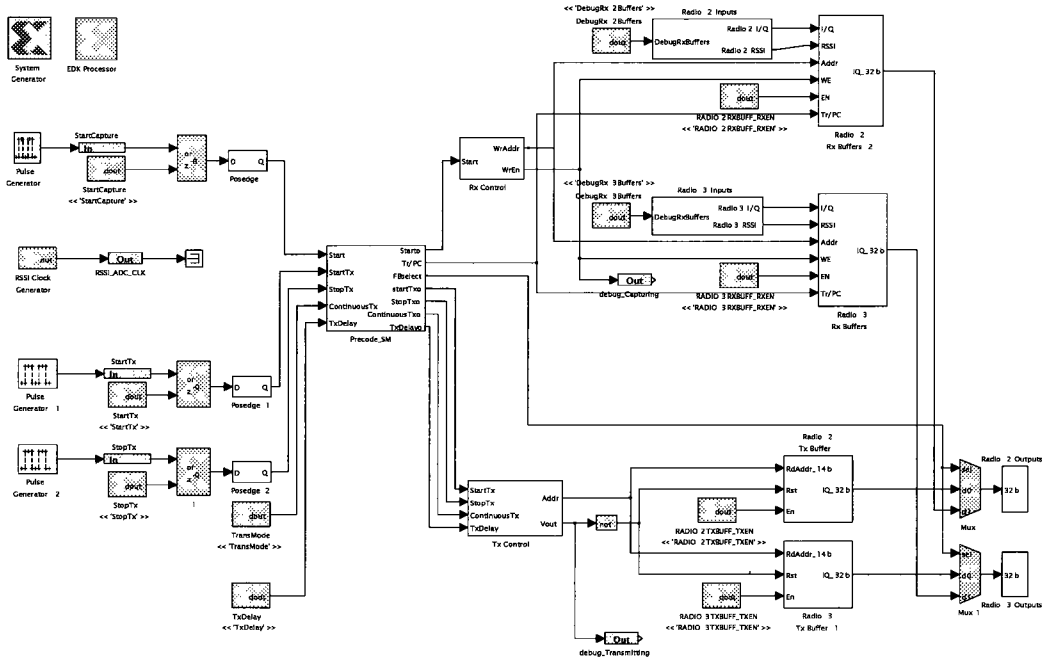

Figure 5.2: Top level EchoWARPLab 2x2 hardware design

State machine

The heart of both the transmitter and receiver consists of a finite state machine designed to execute the two way training algorithm by interleaving round trip training, data and uplink training. The machine transitions to various states as outlined by the state transition diagram in Figure 5.3. The state of the system is fully described by four counters and a bit that is set when in the wait state. The initial values of D, U and X are set prior to an experiment, their initial values are the number of times

a complete training cycle will be completed, the number of uplink training cycles between round trip training and the number of data cycles between uplink training respectively. R is the address counter for the appropriate transmit or receive RAM and is initialized to 2^{14} upon entering the states *Fwd Train*, *Reverse Train* and *Data*. In all states but *Wait* the counter R decrements every 25ns. The inputs to the state machine are START_ECHOTX and START_ECHORX. When one of these inputs is asserted the machine transits from *Wait* to *Fwd Train* on the next clock cycle.

The actions taken by a transceiver in a current state is enumerated in Table 5.2. Once the current state and inputs satisfy a transition rule a state transition is made, and the state machine pauses for a period listed in Table 5.3. These pauses are inserted to allow for settling time of the transceiver IC when switching between TX and RX as outlined in [9] and to allow computation of the channel estimates and programming of the precoder filter weights.

Table 5.2: Transceiver actions during various states

State	**Base Station**	**Mobile Station**
Wait	Waiting for sync cmd	Waiting for sync cmd
Fwd Train	TX Fwd Training	Buffer Fwd Training
Return Train	RX Return Train, form $\widehat{h * g}$	TX Return Training
Reverse Train	RX Reverse Train, Form $\hat{h}$	TX Reverse Train
Data	Precode and TX Data	Receive Data

Table 5.3: Wait times between states

Current State	**Next State**	**Wait time (μs)**
Wait	Fwd Train	0
Fwd Train	Return Train	30
Return Train	Reverse Train	0
Reverse Train	Data	100
Data	Data	0
Data	Reverse Train	30
Data	Fwd Train	30
Data	Wait	0

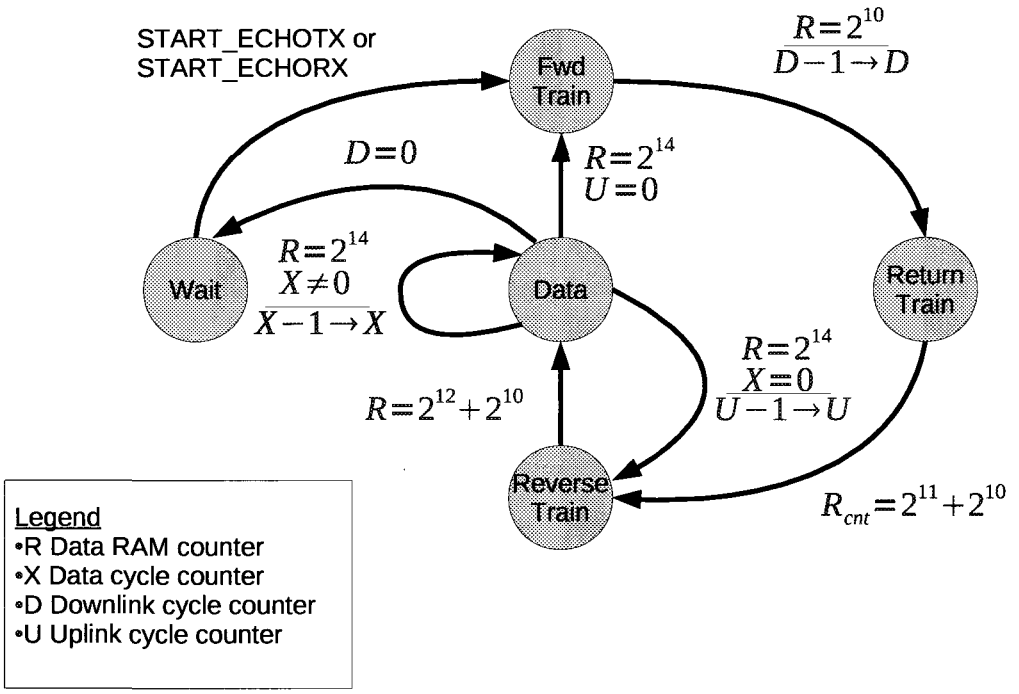

Figure 5.3: FSM diagram

Channel Estimate

During the return training and reverse training phase the base station receives 2^{14} training samples from the mobile. these samples consist of 4096 samples of round trip training originating at antenna 1 of the base station, 4096 that originate from antenna 2 and 8192 sample of uplink training. There has been a great deal of research on the design of channel estimation algorithms, for this work we implement a simple scheme for the frequency selective channel. For the L tap channel we need at least L training symbols for each antenna pair. The training sequence consists of a single symbol followed by $2L$ silent symbol periods. This sequence is repeated with period $2L+1$ for the entire training phase. This sequence when received is a noisy copy of the channel pulse response repeated every $2L+1$ symbol times. The individual pulse

response sequences are summed together so that the noise may be averaged out.

The pulse responses of the round trip training and uplink training are the estimates for $\widehat{h * g}$ and $\hat{g}$ respectively. To form the estimate of the downlink channel we must deconvolve the downlink and uplink channel estimate. This is easily accomplished in the frequency domain and is achieved by a fast Fourier transform and cordic divider.

Precoder

The precoder implemented in this work is that presented in the previous chapter. This system consists of a three tap zero-forcing equalizer for each of the two transmit antennas and a beamforming precoder. Matrix inversion is done with a brute force manner since the matrix in question is only 3×3. For channels with longer impulse responses and subsequently longer zero-forcing filters more efficient matrix inversion such as QRD-RLS method outlined in [22] and [23] would be necessary for a practical system.

Symbol/Carrier Recovery

The first block in the receiver is the system to recover symbol timing. The symbol timing problem is one of selecting the appropriate moment to sample the output of a matched filter. For this work we select an 8 branch interpolating polyphase filter. This method of symbol timing recovery is outlined in [24].

Hard Decision

The hardware that makes a hard decision is pictured in Figure 5.5. The square QAM decision regions allow the simple slice operation to produce the decision making the operation essentially free in terms of resource usage. Since no effort to mitigate ISI is performed at the reciever this simple hard decision represents a receiver archetecture as simple as one designed with only additive noise in mind.

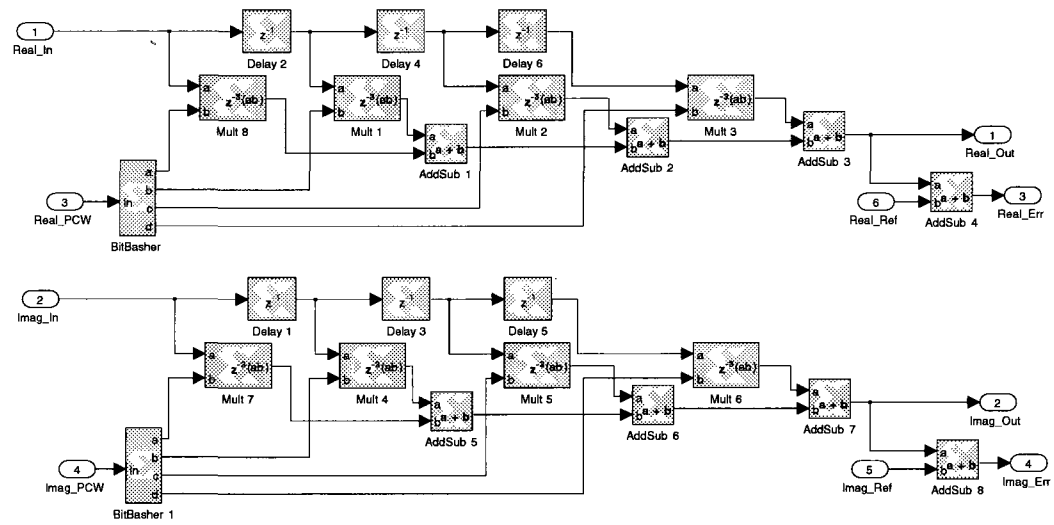

Figure 5.4: Precoder

BER counter and SNR estimate

The BER counter and SNR estimator are included in the receiver hardware to gather experimental results. Since this hardware is only used to measure the system under test it is not considered in the resource utilization number presented below. Each of the received symbols that have been subject to a hard decision by the previous block is compared to the reference data sequence by an xor operation. The output of the xor is the Hamming weight between $\hat{x}$ and x. The hamming weights for every symbol in a data frame are summed to provide the total number of bits in error for that frame. The system measures the average magnitude of the input when the transmitter is known to be silent to calculate the noise power and similarly, the average power when valid data is being received to estimate signal power. The sum of bit errors, average

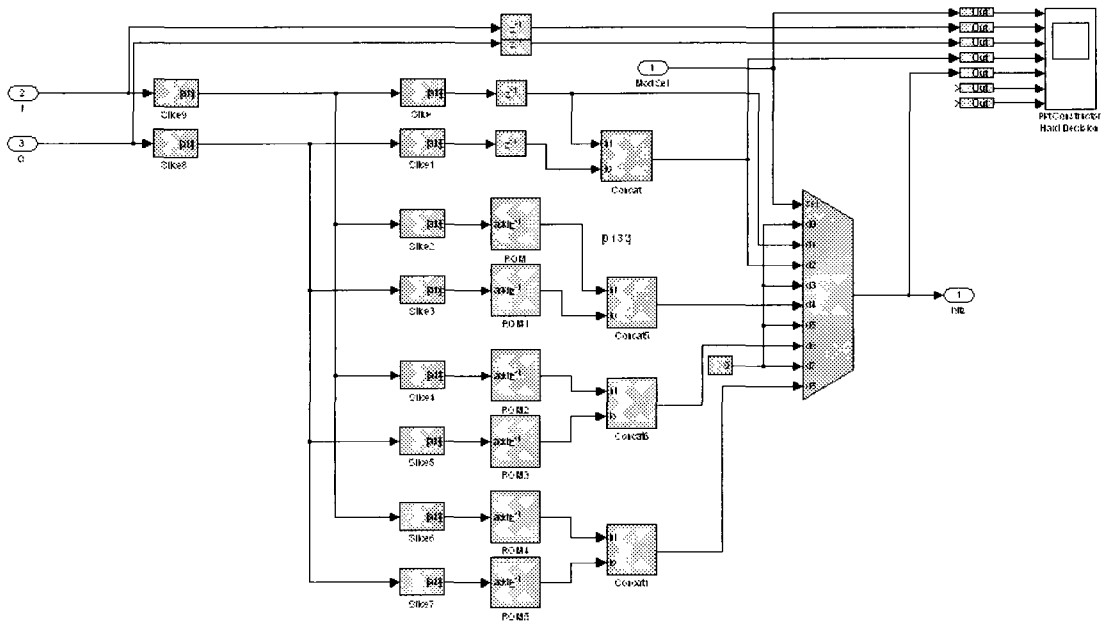

Figure 5.5: Hard Decision

noise power and average signal power are stored in a block RAM for offline processing upon conclusion of an experiment.

5.2 Device Utilization

A major motivation for this work is to shift computational complexity that results in hardware costs and energy consumption from mobile stations to base stations. In this section we present resource utilization numbers for our receiver versus several reference architectures. Our method of shifting equalization and channel estimation to the base station increases the device utilization at the base station since the base station must additionally deconvolve the downlink and uplink CIRs. Deconvolution requires $O(n^2)$ operation however we will not address this added complexity at the

base station for two reasons. First, frequency selective channels in practice are less than 10-20 taps long in the worst case therefore, n is small. Second, the base station is assumed to be relatively unconstrained in terms of computational power.

For a given receiver architecture one of the biggest factors that determine device utilization is the data type of the input signals. IEEE 754 floating-point data types allow a large dynamic range at the price of a complex architecture to process the mantissa and exponent [25]. Fixed point representation is simpler and possesses sufficient dynamic range for many receiver architecture. The WARP radios used to prototype transceivers have 14 bit analog to digital converters for both inphase and quadrature components of the baseband samples. A thorough treatment of the effects of quantization is presented in [26]. Receiver resource utilization for various base band fixed point word lengths is given in Table 5.4. Each system was designed using Xilinx System Generator. The systems designed for 14 bit word length were synthesized, and the utilization results represent actual devices usage. For other word lengths a post routing estimate was obtained from the System Generator tool. From these results we make the observation that both the precoded system and the system utilizing the Alamouti technique are phase coherent communication however the precoded system is a simple as the non coherent DQAM.

Table 5.4: Receiver resource utilization

Word length	**Precoded System**		**DQAM**		**Alamouti**	
	Slice	Mul	Slice	Mul	Slice	Mul
fix16_15	440	4	460	4	1930	16
fix14_13	**390**	**4**	**420**	**4**	**1800**	**16**
fix12_11	350	4	375	4	1675	12
fix10_9	320	4	345	4	1550	12
fix8_7	265	4	315	4	1220	12
fix6_5	210	4	255	4	1120	12
fix4_3	140	4	190	4	870	12

CHAPTER 6

Experiment Setup and Results

While there has been many works that propose models or methods for utilizing symmetry in the wireless channel there is a lack of empirical evidence to substantiate the assumption of symmetry in wireless channels. In this section we present experimental results that show first, that two-way wireless communication in an office environment experiences a symmetric channel with the exception of the RF front ends of the transceivers and second, that the coherence time of the RF front ends is orders of magnitude longer than that of the wireless channel. The two-way training, channel estimation and precoding scheme outlined in the previous chapters is compared with a non-coherent downlink that utilizes DQAM and a coherent system utilizing the Alamouti coding technique. Our results show that in an office environment our schemes BER performance is similar to the Alamouti technique and strictly outperforms DQAM. Furthermore, we show that our systems receiver is significantly simpler than the system utilizing the Alamouti technique and about the same complexity of DQAM. Succinctly, in terms of BER vs receiver complexity our system outperforms the existing methods we benchmark against.

This chapter is outlined as follows. In Section 6.1 a comparison of forward channel estimates is made between that obtained at the base station from round trip training

and that at the mobile station from forward training. Section 6.2 details the systems we compare our round trip training and precoding against. We conclude this chapter with Section 6.3 where round trip training and precoding are evaluated against the reference systems in terms of receiver complexity and BER.

6.1 Experimental Investigation of CIR

In an effort to validate the assumption of a symmetric wireless channel the following experiment was performed on a SISO system. The round trip training protocol was executed once every 500ms and the resulting received training symbols at the base station and mobile that were then collected on the host computer for off-line processing. Training was conducted for a two minute period yielding 240 sets of training symbols from both stations. This experiment was performed twice in two separate settings. First, in an office with the mobile and base station located such that a line of sight path existed at a range of 2 meters. Second, in the open area of Duncan Hall at Rice University. For the second trial the nodes were placed such that there was no line of sight path. This second trial provided relevant signal paths up to 600 feet resulting in a delay spread that traversed several symbol times resulting in a frequency selective channel. Figures 6.1 and 6.2 plot five sample estimates from both transceivers in the office environment and open area respectively.

For each trial we consider two cases. One where the base station forms an initial estimate $\hat{h}_A$ based on the first set of round trip training. This estimate becomes stale as the channel changes over time resulting in an increasing disparity between the base station and mobile station estimate as measured by the sum over taps of the Euclidean distance between the two estimates. In the second case, the base station periodically updates its estimate with uplink training.

Figure 6.3 plots the sum over time of the Euclidean distance between the base

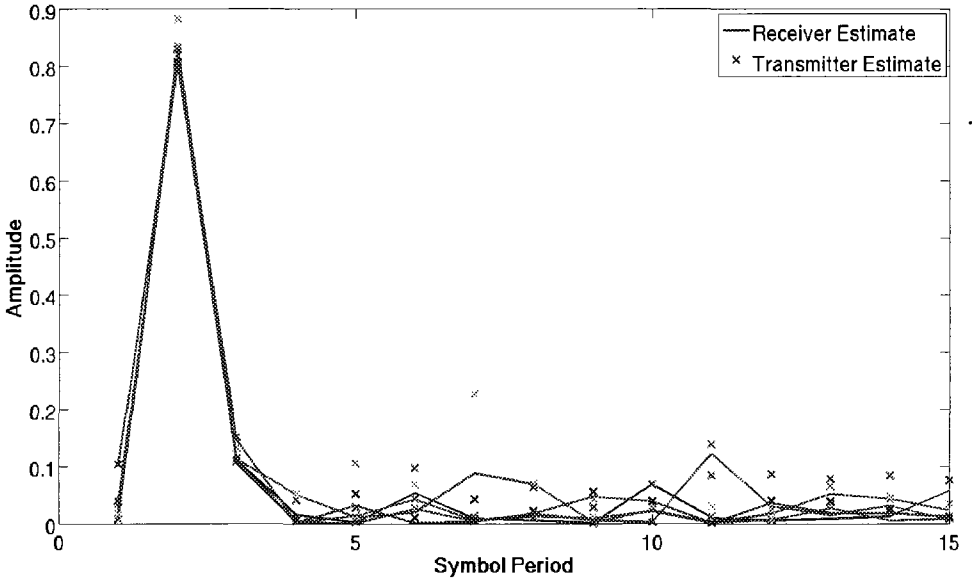

Figure 6.1: $|\hat{h}_A|$ and $|\hat{h}_B|$ for the LOS Office Environment

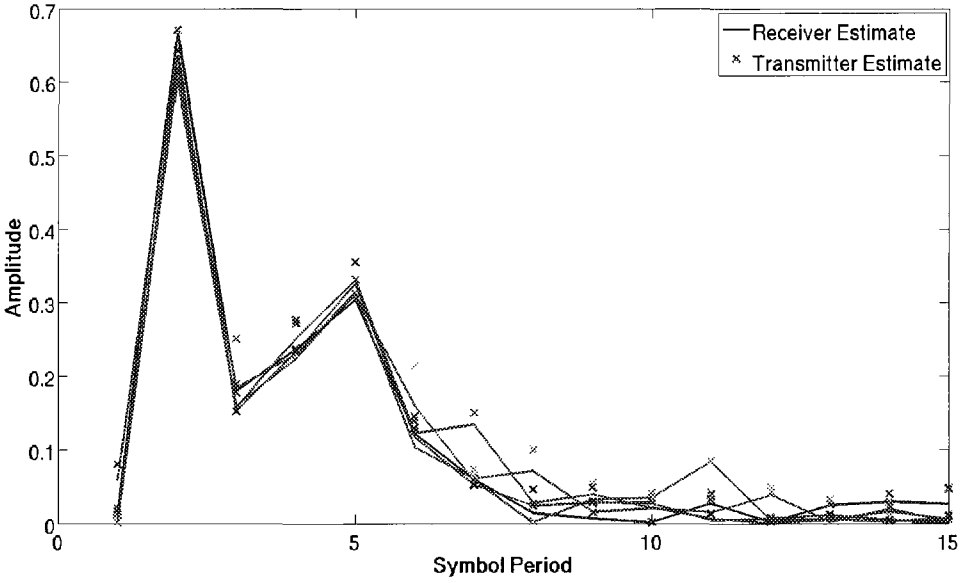

Figure 6.2: $|\hat{h}_A|$ and $|\hat{h}_B|$ for the NLOS Environment

station estimate and mobile station estimate averaged over 500 trials. Each of the channel estimates was normalized such that the sum of magnitude of the tap estimates is unity. These measurements were taken at Duncan Hall in the evening when only occasional pedestrian traffic perturbed the channel. With normalized 16 QAM

modulation the base stations static downlink channel estimate would remain relevant for 60 training periods in this environment while updating the estimate with uplink training extends the relevant period to 180 training periods.

In order to interpret Figure 6.3 we first note that if the channel were completely symmetric then uplink training would sufficient to update the base stations estimate of the forward channel. If this were the case we would expect the normalized average Euclidean distance to reset to about 0.04 each time reverse training was performed. Conversely, if the uplink and downlink channels were completely uncorrelated the uplink training would provide no additional information for our estimate and we would expect the distance would be no better than the case with no uplink training.

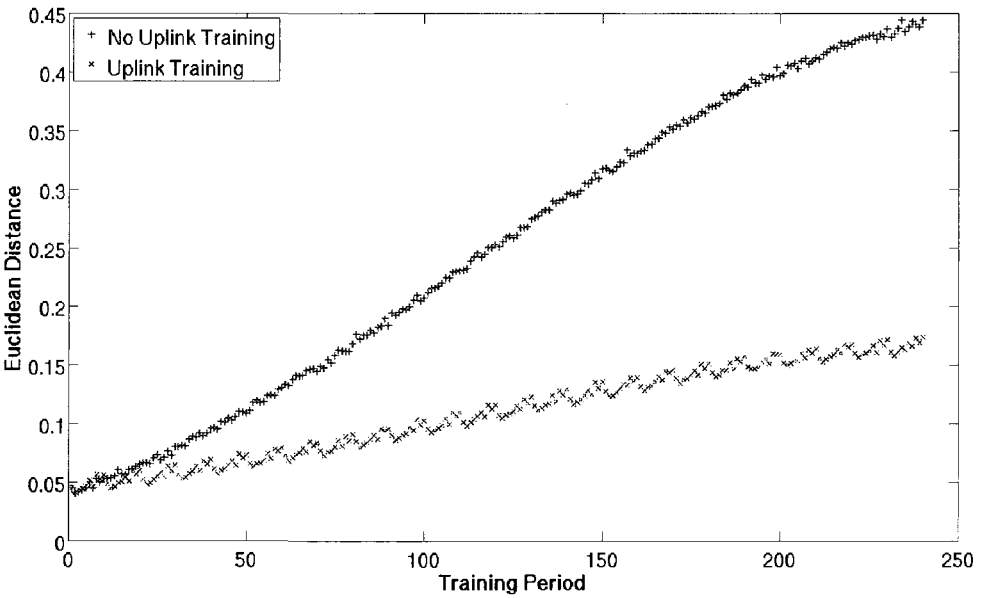

Figure 6.3: $\sqrt{\sum_L (\hat{h}_A - \hat{h}_B)^2}$ vs. time since initial training

6.2 Reference Designs

The receiver complexity and BER performance of the system utilizing round trip training and precoding is compared against two reference designs. Both of the ref-

erence designs do not require round trip training so they may be implemented in WARPLab where signal processing concerning the fading channel and symbol decision can be performed off line using MATLAB on the host computer. Symbol timing for each of the reference designs is recovered initially from a three symbol BPSK preamble at the start of each TDD frame and maintained by a Costas loop.

6.2.1 Differential Quadrature Amplitude Modulation

Differential quadrature amplitude modulation differers from other modulation schemes considered in this thesis by modulating the *change* QAM symbols modulating the carrier rather than simply modulating phase and amplitude as in QAM. Since data is conveyed by the change rather than the absolute phase of the received signal no phase reference is needed at the receiver. The receiver possesses no hardware for phase recovery nor does it posses channel estimation and equalization. As noted in the Section 5.2 the complexity of this receiver is similar to the precoded system however, it possesses no capability to exploit transmit diversity of the MISO channel and suffers from unmitigated ISI when encountering a frequency selective channel.

6.2.2 Alamouti Codes

A technique that achieves full diversity for the 2×1 MISO, flat fading channel is presented in [27]. With the modifications to Alamouti's original space time codes proposed in [28] it is possible to achieve full diversity in the case where the channel causes ISI. Equalization is accomplished with the same order zero-forcing equalizer as utilized in the precoded system and channel estimates are obtained by the same forward training sequence that a mobile station in the precoded system would echo back to the base station.

The similarity of the equalizer in this scheme and the precoder make this system the most comparable to the precoded system. The difference in the two systems

is simply that the channel estimation and equalization have been shifted from the mobile station to the base station. This system achieves diversity with space time coding while the precoded system achieves diversity though beamforming. This system requires no feedback unlike the precoded system but suffers a 3dB penalty versus a system with CSIT as noted by Alamouti.

6.3 Bit Error Rate and Complexity

The precoded system is compared against the reference systems in terms of BER in Figure 6.5. These results were obtained via the experiment setup pictured in Figure 6.4. The channel emulator was programmed to emulate a pedestrian model slow fading channel experiencing NLOS and a delay spread of 100ns. The channel gain was modulated across trials to sweep SNR and the received SNR for each trial was estimated at the receiver.

These results show that while the precoding system strictly outperforms the Alamouti system when channel information is perfect this is not always the case when the channel state must be estimated. In low to medium SNR precoding strictly outperforms Alamouti and both perform better than DQAM. At high SNR, above about 20dB, the Alamouti scheme performs best with precoding slightly better than halfway between DQAM and Alamouti in terms of BER.

We noted in the previous chapter that the fixed-point word length of the demodulated signal is a key parameter of the resource utilization at the mobile station. The fixed point processing introduces quantization error for which the magnitude of the error on average is a function of the word length. Figure 6.6 plots BER vs. word length for various systems operating at a fixed SNR with 16 QAM modulation. Succinctly, this plot shows that for this particular modulation order representing the inphase and quadrature components with more than about 7 bits yields little im-

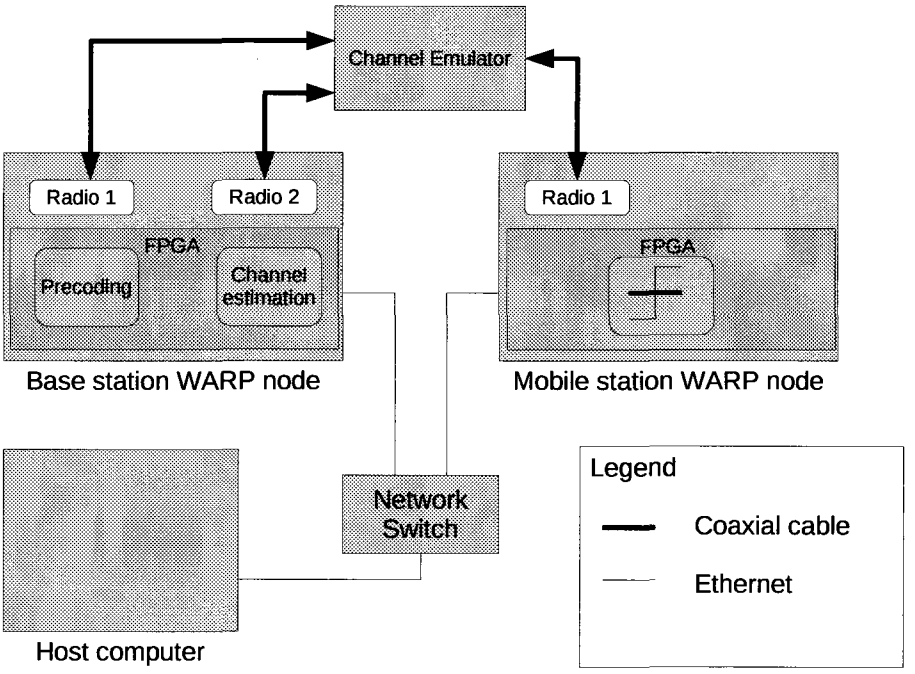

Figure 6.4: Block diagram of channel emulator experiment

provement as the error from quantization becomes vanishingly small as errors from the channel dominate. Since resource utilization at the receiver is so strongly dependent on word length this result leads us to the next result which examines BER vs the mobile station receiver size.

The results in Figure 6.7 are the culminating point of this section and of this thesis. This plot compares the bit error rate with the number of slices in the receiver architecture dedicated to channel estimation, equalization and symbol level decision for various receiver configurations. This plot contains information about the two metrics of interest in this work, BER and receiver complexity. In terms of these metrics, in this figure, systems plotted in the lower left are desirable while systems on the upper right are not. To parse the results in this figure we note that on the

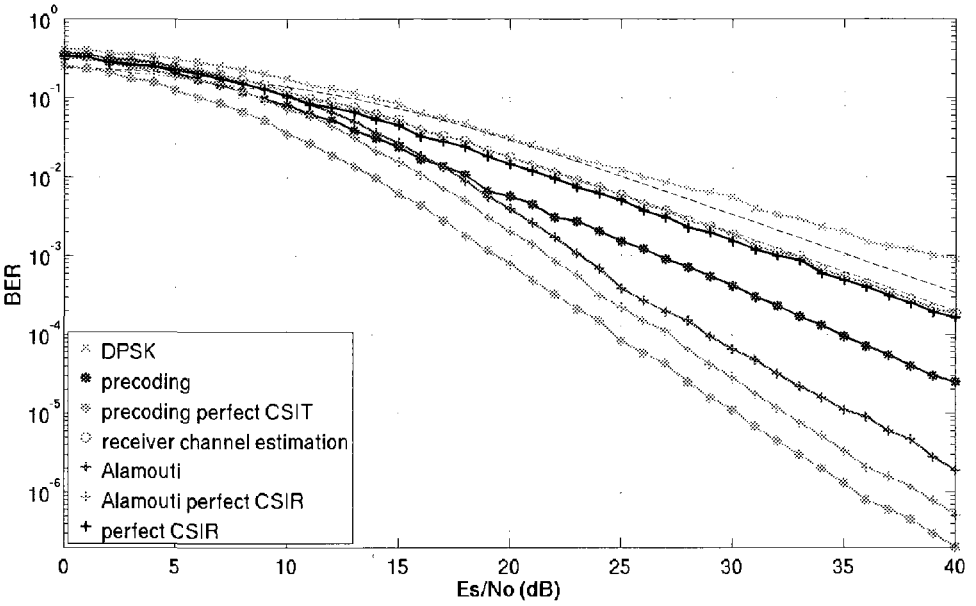

Figure 6.5: Bit error rate vs. signal to noise ratio

left side of the figure receivers designed to process DQAM, precoding and the AWGN channel all require a similar number of resources. Phase coherent communication systems that require channel estimation and equalization at the receiver are plotted on the right, each of these require about the same amount of resources. We note that the receiver utilizing the precoding scheme achieves a bit error rate similar to that of the Alamouti scheme but with resource utilization comparable to systems that do not attempt or do not need to account for phase ambiguity.

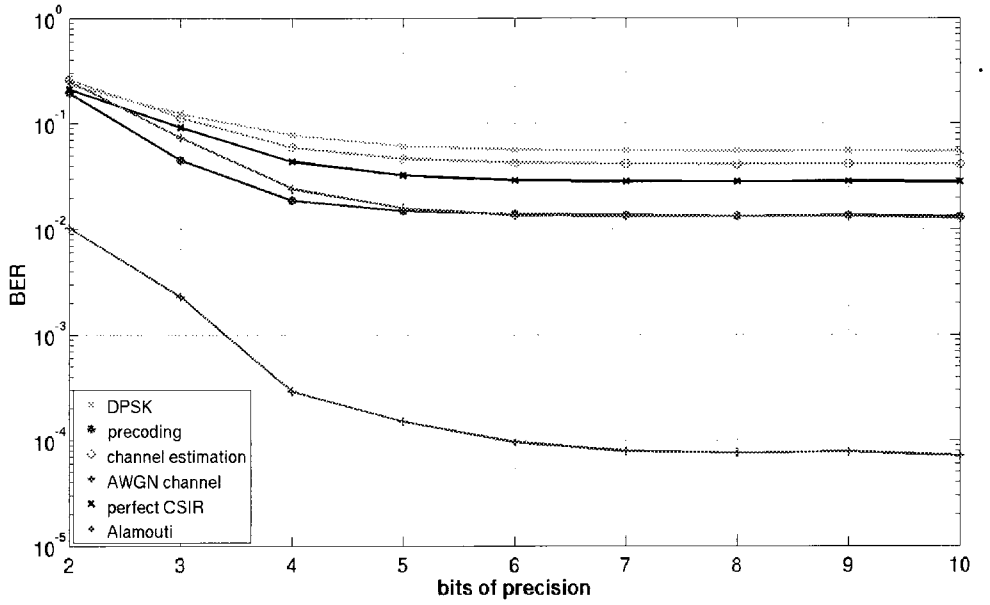

Figure 6.6: Bit error rate vs. baseband fixed-point word length, Receive SNR = 17 dB

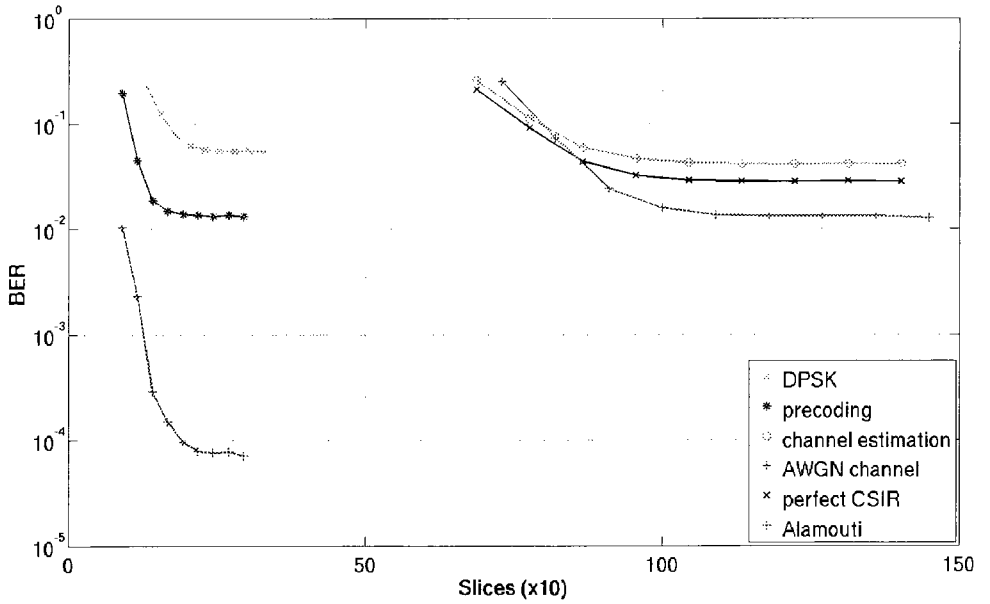

Figure 6.7: Bit error rate vs. mobile station receiver size, Receive SNR = 17 dB

CHAPTER 7

Conclusion

With this work we have outlined a new training and precoding scheme that both leverages the symmetric nature of the wireless channel and exploits the disparity of the coherence times of the wireless channel and RF front ends. The training scheme provides the sufficient statistic for an estimate of the downlink channel at the base station. Periodic uplink training is used to update the base station's downlink channel estimate without inuring the overhead of round trip training. The base station then uses its downlink channel estimate to precoded in a manner that shifts the computational complexity of equalization and carrier recovery from the mobile station to the base station.

Empirical results are presented that demonstrate that an effective channel estimate may be obtained at the base station by way of the proposed training scheme and that when uplink training is utilized to update the downlink channel estimate a better estimate results. The training and precoding scheme are prototyped on the Rice University WARP radio. With this prototype we show that a very simple non-coherent receiver can achieve performance similar to a coherent system with equalization when operating in a slow fading environment.

Bibliography

[1] G. Smith, "A direct derivation of a single-antenna reciprocity relation for the time domain," *Antennas and Propagation, IEEE Transactions on*, vol. 52, no. 6, pp. 1568–1577, June 2004. 1.2

[2] C. Steger, A. Khoshnevis, A. Sabharwal, and B. Aazhang, "The case for transmitter training," *Information Theory, 2006 IEEE International Symposium on*, pp. 35–39, July 2006. 1.2

[3] C. Khoshnevis, A. Sabharwal, B. Aazhang, and C. Steger, "The importance of transmitter side information and the value of training," in *Proc. of Allerton Conference on Communication, Control and Computing*, SEP. 2005. 1.2

[4] M. Guillaud, D. Slock, and R. Knopp, "A practical method for wireless channel reciprocity exploitation through relative calibration," *Signal Processing and Its Applications, 2005. Proceedings of the Eighth International Symposium on*, vol. 1, pp. 403–406, 28-31, 2005. 1.2

[5] L. Withers, R. Taylor, and D. Warme, "Echo-mimo: A two-way channel training method for matched cooperative beamforming," *Signal Processing, IEEE Transactions on*, vol. 56, no. 9, pp. 4419–4432, Sept. 2008. 1.2, 1.5

[6] C. Steger and A. Sabharwal, "Single-input two-way simo channel: diversity-multiplexing tradeoff with two-way training," *Wireless Communications, IEEE Transactions on*, vol. 7, no. 12, pp. 4877–4885, December 2008. 1.3

[7] R. E. Ziemer and R. L. Peterson, "Introduction to digital communication (2nd edition)," 2001. 1.3, 1.4

[8] W. Yu and T. Lan, "Transmitter optimization for the multi-antenna downlink with per-antenna power constraints," *Signal Processing, IEEE Transactions on*, vol. 55, no. 6, pp. 2646 –2660, june 2007. 1.5

[9] *MAX2828/MAX2829 Single-/Dual-Band 802.11a/b/g World-Band Transceiver ICs datasheet (Rev 0)*, 2004. 2.1, 5.1

[10] I. Abou-Faycal, M. Trott, and S. Shamai, "The capacity of discrete-time memoryless rayleigh-fading channels," *Information Theory, IEEE Transactions on*, vol. 47, no. 4, pp. 1290–1301, May 2001. 2.2.1

[11] L. Ozarow, S. Shamai, and A. Wyner, "Information theoretic considerations for cellular mobile radio," *Vehicular Technology, IEEE Transactions on*, vol. 43, no. 2, pp. 359 –378, may 1994. 2.2.2

[12] E. Biglieri, J. Proakis, and S. Shamai, "Fading channels: information-theoretic and communications aspects," *Information Theory, IEEE Transactions on*, vol. 44, no. 6, pp. 2619–2692, Oct 1998. 2.2.2

[13] J. G. Proakis, "Digital communications (4th edition)," 2001. 3.1, 3.1

[14] L. Tong, B. M. Sadler, and M. Dong, "Pilot-assisted wireless transmissions: general model, design criteria, and signal processing," *IEEE Signal Processing Magazine*, vol. 21, no. 6, pp. 12–25, Nov. 2004. 3.1

[15] S. M. Kay, "Fundamentals of statistical signal processing - estimation theroy," 1993. 3.1

[16] B. Hassibi and B. Hochwald, "How much training is needed in multiple-antenna wireless links?" *IEEE Transactions on Information Theory*, vol. 49, no. 4, pp. 951–963, Apr. 2003. 3.3

[17] D. Samardzija and N. Mandayam, "Pilot-assisted estimation of mimo fading channel response and achievable data rates," *Signal Processing, IEEE Transactions on*, vol. 51, no. 11, pp. 2882 – 2890, nov 2003. 3.3

[18] D. Palomar and M. Lagunas, "Joint transmit-receive space-time equalization in spatially correlated mimo channels: a beamforming approach," *Selected Areas in Communications, IEEE Journal on*, vol. 21, no. 5, pp. 730 – 743, june 2003. 4

[19] E. Visotsky and U. Madhow, "Space-time transmit precoding with imperfect feedback," *Information Theory, IEEE Transactions on*, vol. 47, no. 6, pp. 2632–2639, Sep 2001. 4

[20] R. Badra and B. Daneshrad, "Asymmetric physical layer design for high-speed wireless digital communications," *Selected Areas in Communications, IEEE Journal on*, vol. 17, no. 10, pp. 1712–1724, Oct 1999. 4

[21] http://warp.rice.edu/trac/wiki/WARPLab. 5.1

[22] M. Karkooti, J. Cavallaro, and C. Dick, "Fpga implementation of matrix inversion using qrd-rls algorithm," 28 - November 1, 2005, pp. 1625 – 1629. 5.1

[23] J. Eilert, D. Wu, and D. Liu, "Efficient complex matrix inversion for mimo software defined radio," may 2007, pp. 2610 –2613. 5.1

[24] F. Harris and M. Rice, "Multirate digital filters for symbol timing synchronization in software defined radios," *Selected Areas in Communications, IEEE Journal on*, vol. 19, no. 12, pp. 2346 –2357, dec 2001. 5.1

[25] C. Doss and J. Riley, R.L., "Fpga-based implementation of a robust ieee-754 exponential unit," april 2004, pp. 229 – 238. 5.2

[26] G. B. Middleton, "On the impact of receiver quantization on the performance of wireless communication systems," 2007. 5.2

[27] S. Alamouti, "A simple transmit diversity technique for wireless communications," *Selected Areas in Communications, IEEE Journal on*, vol. 16, no. 8, pp. 1451 –1458, oct 1998. 6.2.2

[28] E. Lindskog and A. Paulraj, "A transmit diversity scheme for channels with intersymbol interference," vol. 1, 2000, pp. 307 –311 vol.1. 6.2.2